Title

Intrinsic aggregation and propagation of unmodified tau peptides: R2R3 as a minimal model system

Authors

Viswanath Das[1,2], Luisa Diomede[3], Lukáš Malina[1,4], Michele Mosconi[3], Narendran Annadurai[1]

Affiliations

[1] Institute of Molecular and Translational Medicine, Faculty of Medicine and Dentistry, Palacký University and University Hospital Olomouc, Hněvotínská 1333/5, 779 00 Olomouc, Czech Republic

[2] Czech Advanced Technologies and Research Institute (CATRIN), Institute of Molecular and Translational Medicine, Palacký University Olomouc, Křížkovského 511/8, 779 00, Olomouc, Czech Republic

[3] Department of Molecular Biochemistry and Pharmacology, Istituto di Ricerche Farmacologiche Mario Negri IRCCS, Via Mario Negri 2, 20156 Milan, Italy

[4] Department of Medical Biophysics, Faculty of Medicine and Dentistry, Palacký University Olomouc, Hněvotínská 3, 775 15, Olomouc, Czech Republic

Corresponding author

Viswanath Das (ORICID: 0000-0001-5973-5990)
Institute of Molecular and Translational Medicine
Faculty of Medicine and Dentistry
Palacký University and University Hospital Olomouc
Hněvotínská 1333/5, 779 00 Olomouc, Czech Republic
Email: viswanath.das@upol.cz; Tel.: +420 585 632 243, Fax: +420 585 632 180

Running title: R2R3 as a minimal tauopathy model

Keywords

Amyloid fibrils; Prion-like propagation; Seeding activity; Tauopathy; Tau aggregation

Abstract

Tau aggregation into neurofibrillary tangles is a defining feature of Alzheimer's disease and other tauopathies. Although aggregation depends largely on specific amyloidogenic motifs (particularly VQIINK and VQIVYK) in repeated regions of tau microtubule-binding domain, how the primary sequence of adjacent repeats intrinsically influences aggregation and prion-like propagation remains unclear. This study systematically characterized three unmodified, physiologically relevant tau peptide constructs -R1R3, R2R3, and R3R4 - to define their intrinsic aggregation kinetics, structural features, and prion-like seeding activity. Among these constructs, we found that R2R3 showed rapid aggregation, distinct β-sheet formation, and potent seeding capable of sustained secondary propagation in cellular biosensor assays. While recent studies have highlighted chemically modified peptides (e.g., acetylated and phosphomimic peptides), our study emphasizes the importance of native, unmodified sequences as fundamental determinants in tau aggregation. Furthermore, these findings establish R2R3 as a robust minimal tau model, providing a valuable tool for mechanistic research and therapeutic screening in tau-related neurodegeneration.

Statement of Significance

Tauopathies involve pathological tau aggregation and propagation, but the minimal tau sequences capable of initiating and spreading aggregation remain unclear. This study identifies the tau fragment R2R3 as intrinsically capable of rapidly forming stable, β-sheet-rich fibrils and effectively inducing sustained intracellular aggregation. Critically, our results show that the native R2-R3 junction alone, without introduced modifications, is sufficient for robust tau aggregation and seeding activity, revealing a previously unrecognized minimal element responsible for tau pathology. This provides a streamlined experimental model for studying fundamental tau aggregation mechanisms and screening therapies targeting events associated with initial tau assembly.

Introduction

Tau is a key microtubule-associated protein that stabilizes microtubule structure and is essential for maintaining neuronal integrity and intracellular transport. Under pathological conditions, tau undergoes abnormal modifications, such as hyperphosphorylation and truncation, leading to its

detachment from microtubules and subsequent aggregation into insoluble amyloid fibrils (1). These aggregates form the neurofibrillary tangles (NFTs) that are a hallmark of tauopathies, including Alzheimer's disease (AD) and frontotemporal dementia.

The aggregation of tau is driven by the amyloid-prone hexapeptide motifs, VQIINK and VQIVYK, located in the N-terminal part of repeats R2 and R3 within the microtubule-binding domain (2). Cryo-electron microscopy studies of tau filaments extracted from AD brains have resolved a common fibril core composed predominantly of R3 and R4, arranged in a cross-β architecture with disease-specific polymorphisms (3). Molecular dynamics simulations and structural studies have confirmed that VQIVYK and VQIINK form steric zipper interfaces that drive β-sheet assembly (4).

Under physiological conditions, tau aggregation is regulated by local sequence context and structural motifs that shield amyloidogenic motifs. Stabilizing β-turn elements and proline-glycine-glycine-glycine motifs reduce aggregation by limiting access to VQIVYK and VQIINK (5). Disease-associated mutations, such as P301L, and alternative splicing that modulate tau repeat composition can disrupt these protective features and promote aggregation (5, 6). Furthermore, cysteine residues within repeat domains, particularly C322 in R3, contribute to oligomerization and fibril stability via disulfide crosslinking (7).

Significant insights into tau aggregation mechanisms have emerged over the past two decades. Early investigations demonstrated differential intrinsic aggregation propensities between the VQIVYK and VQIINK motifs, highlighting VQIVYK as a particularly potent fibrillization driver (2). Building on these findings, later studies revealed that full-length tau adopts conformational ensembles with structural features that naturally shield amyloidogenic motifs from aggregation (5). These observations are further supported by studies that identified VQIVYK as part of the first intermediate amyloid in the assembly of disease-specific tau polymorphs (8). Recently, it has also been demonstrated that isolated PHF6 peptides can form polymorphic fibril structures (4), underscoring the relevance of minimal peptide models for dissecting tau aggregation pathways. Recent findings indicate that post-translational modifications - especially lysine acetylation proximal to amyloidogenic motifs - can significantly enhance fibril stability and aggregation (9). These motifs have also become valuable therapeutic targets, as evidenced by peptide inhibitors and epitope-specific antibodies that selectively modulate tau aggregation (10–12).

Despite these developments, the intrinsic aggregation properties of physiologically relevant, unmodified tau repeat peptide constructs remain incompletely characterized. Recent studies provided critical insight into chemically modified (acetylated and phosphomimic) tau peptides (9, 13). Yet, it is still a matter of debate whether the key determinants for tau amyloid assembly and prion-like behaviors are intrinsically encoded into the primary sequence of repeated regions or reside in post-translational modified residues. To address this gap, we systematically characterized three unmodified tau peptide constructs, R1R3, R2R3, and R3R4, representing native repeat combinations found in 3R and 4R tau isoforms. Specifically, we sought to define their intrinsic aggregation kinetics, structural polymorphisms, and seeding potentials, establishing a crucial biochemical foundation for future comparative analyses involving chemical modifications, disease-associated mutations, and therapeutic approaches.

Methods

Materials

Peptides (purity >95%) were custom-synthesized by ProteoGenix (Schiltigheim, France). The peptides were solubilized in ultra-pure water, aliquoted in smaller portions to minimize freeze-thaw cycles, and stored at -80°C. Before use, peptides were thawed on ice and then briefly centrifuged at 12,100 × g for 1 min using a Mini Spin Plus 5453 Centrifuge (Eppendorf, Hamburg, Germany).

Tau aggregation and hydrophobic residues characterization

Tau peptide aggregation and the exposure of hydrophobic residues were monitored using Thioflavin T (ThT) and 8-anilino-1-naphthalenesulfonic acid (ANS) fluorescence assays, respectively. Briefly, reactions (40 µL total volume) containing 25-50 µM peptide, 15 µM ThT (Sigma-Aldrich; Cat. # T3516-5G), or 40 µM ANS (Sigma-Aldrich, Cat. # A1028-5G), and 5 µM heparin (Sigma-Aldrich; Cat. # H4784–1G) were prepared in aggregation buffer [20 mM Tris (pH 7.4), 100 mM NaCl, 1 mM EDTA]. Reaction mixtures were immediately aliquoted into clear-bottom black 384-well ViewPlates (Revvity; Part # 6007460), sealed with TopSealA-PLUS (Revvity) to prevent evaporation, and incubated at 37°C in an EnSpire Multimode Plate Reader (Revvity). Samples were continuously agitated (1000 rpm), with an upper heater temperature set 2°C above the lower heater to prevent condensation. Fluorescence intensity (ThT: Ex: 460-490

nm, Em: 500-550 nm; ANS: Ex: 390 nm, Em: 475 nm) was measured every 10 min over 72 h or every 12 h for 168 h.

Atomic force microscopy

To visualize fibril morphology at 48 and 168 h post-aggregation, atomic force microscopy (AFM) was performed. Aggregated peptide samples were deposited onto freshly cleaved mica substrates (10 mm, Ted Pella, Inc., Redding, CA, United States) and air-dried at room temperature for 10 min. Following deposition, each mica surface was gently rinsed five times using sterile deionized water and air-dried for 10-15 min. These were then fixed onto glass slides using transparent adhesive tape for stabilization during imaging.

AFM imaging was performed using an Olympus IX81 microscope with a Veeco BioScope™ Catalyst™ system (Bruker, Billerica, MA), as described before (14), using the SCANASYST AIR probe (tip radius: 2 nm, spring constant: 0.4 N/m). Raw images were processed and analyzed using NanoScope Analysis 1.9 (Bruker).

Hydrophobicity Analysis

Hydropathy profiling of tau repeat peptides (R2R3, R1R3, and R3R4) was performed using the Kyte-Doolittle scale implemented via the ProtScale tool available on ExPASy (15). The analysis used a window size of 9 (default), with linear weight variation and 100% relative edge weighting. Positive values indicate hydrophobic residues, while negative values indicate hydrophilic residues. Minimum and maximum hydropathy scores and the corresponding residue positions were extracted to identify local hydrophobic and hydrophilic domains. These parameters were compared across peptides to evaluate correlations with their aggregation behaviors.

SDS-PAGE and Western blotting

Aggregated peptide samples (50 μM, with 5 μM heparin) were prepared in parallel to ThT assays under identical buffer and incubation conditions but without ThT. For Coomassie-stained gel analysis, samples were mixed with 4× NuPAGE™ LDS Sample Buffer (ThermoFisher, Cat. # NP0008) without reducing agent, heated at 70 °C for 10 min, and loaded onto NuPAGE™ 4–12% Bis-Tris gels (Invitrogen, Cat. # NP0335BOX). Electrophoresis was performed using NuPAGE™ MES SDS Running Buffer (ThermoFisher, Cat. # NP0002) under non-reducing conditions. Gels were fixed in 50% methanol and 10% acetic acid for 1 h, stained overnight at 4°C with Coomassie

Brilliant Blue R-250 staining solution (Bio-Rad, Cat. # 1610436EDU), and destained in deionized water. Gel images were acquired using a ChemiDoc MP imaging system (Bio-Rad).

For Western blotting, aggregated samples were mixed with 2× Laemmli buffer [62.5 mM Tris-HCl (pH 6.8), 25% glycerol, 2% SDS, 0.01% bromophenol blue, and 5% β-mercaptoethanol], boiled for 5 min at 95°C, and resolved by SDS-PAGE on Mini-PROTEAN TGX 4-20% precast gels (Bio-Rad, Cat. # 4561095) using Tris/Glycine/SDS running buffer. Proteins were transferred to PVDF membranes using the Trans-Blot Turbo Transfer System (Bio-Rad). Membranes were blocked in 5% BSA in 1× TBST (0.1% Tween® 20) for 1 h at room temperature, incubated overnight at 4°C with anti-Tau (4-repeat isoform RD4) antibody, clone 1E1/A6 (1:1000; Millipore Cat. # 05-804, RRID: AB_310014), and then with Alexa Fluor 488-conjugated anti-mouse secondary antibody (1:2000; Invitrogen, Cat. # A21202) for 1-2 h at room temperature in the dark. Bands were visualized using the ChemiDoc MP imaging system (Bio-Rad).

Circular dichroism spectroscopy

Tau peptides at 5 and 10 μM concentrations were diluted in 10 mM phosphate buffer (PB), pH 6.8, either alone or with heparin at a 5:1 peptide-to-heparin molar ratio. Samples were incubated at 37 °C, and the circular dichroism (CD) spectra were recorded immediately after sample preparation (T0) and 24 and 48 h later using a Jasco J-815 spectropolarimeter (Jasco). Spectra were measured from 195 to 260 nm (bandwidth 1.0 nm; resolution 0.1 nm) in a quartz cuvette with a 0.1 cm path length. Sensitivity was set to 100 mdeg, the scan rate was 100 nm/min, the response time was 4 s, and the spectra were averaged from five measurements. Results were expressed as mean molar ellipticity after subtracting background PB spectra.

Biosensor cell seeding assay

Peptide aggregates prepared without ThT were collected after 48 h or 168 h of aggregation and pooled to make a 120 μL final volume. Total protein concentrations of aggregated samples were measured by Pierce™ BCA Protein Assay Kit (Thermo Fisher Scientific; Cat. # 23225). Aggregates were standardized to 100 nM concentration and fragmented by ultrasonication using a Branson Ultrasonic Sonifier (Marshall Scientific, Hampton, NH) at 30% amplitude, with 15 s ON/OFF intervals for 1 min.

Tau RD P301S FRET Biosensor cells were obtained from ATCC (Manassas, VA, USA) and maintained in DMEM high-glucose (4.5 g/L; Lonza; Cat. # 12-604F), supplemented with 10% fetal bovine serum (Gibco; Cat. # A5256701), 1% penicillin-streptomycin (Thermo Fisher Scientific; Cat. # 15140163), 1 mM GlutaMAX™ (Thermo Fisher Scientific; Cat. # 35050061) and 10 mM HEPES buffer (Serana Europe; Cat. # BSL-001-100ML). Cells were routinely cultured at 37°C in a humidified incubator with 5% CO_2, passaged every 3-4 days upon reaching ~80% confluency, and regularly tested for mycoplasma contamination.

For seeding assays, cells were seeded at 5×10^3 cells per well in poly-D-Lysine-coated, black optically clear-bottom PhenoPlate 384-well plates (Revvity; Part # 6057302). Cells were returned to the incubator for overnight cell attachment. The following day, cells were seeded with 100 nM fibrillar aggregates mixed with 0.2 µL/well TurboFect™ Transfection Reagent (Thermo Fisher Scientific; Cat. # R0533) in 10 µL Opti-MEM™ medium (Thermo Fisher Scientific; Cat. # 11058021) for 72 h at 37°C. After the end of the seeding assay, cells were fixed using 2% paraformaldehyde (Electron Microscopy Services; Cat. # 15714-1L) for 10 min at room temperature, washed with PBS, and stained with Hoechst-33342 (10 µM; Invitrogen, Cat. # H21492). To preserve cells for imaging, 1% glycerol was added per well.

Cell fractionation and reseeding assay

Triton X-100 soluble and insoluble fractions were prepared as described (14). Briefly, cells following 72 h of seeding with fibrillar aggregates, as described in the previous section, were lysed in 1x Tris-buffered saline containing 0.05% Triton X-100 and protease/phosphatase inhibitors (Roche; Cat. # 04693116001 and Cat. # 04906837001). After centrifugation at 1,000 × *g* for 10 min (4°C), the supernatants were further ultracentrifuged at 24,400 × *g* for 1 h to separate soluble from insoluble fractions. The insoluble pellets were resolubilized in RIPA buffer (Thermo Fisher Scientific; Cat. # 89901) containing protease/phosphatase inhibitors.

Subsequently, reseeding assays were conducted by plating biosensor cells at 5×10^3 cells per well in poly-D-Lysine-coated plates, as described in the previous section. The next day, cells were transfected with either total, soluble, or insoluble fractions (1 µg per well). The medium was replaced after 24 h, and cells were further incubated at 37°C for 48 h before imaging.

Imaging and quantification

High-content imaging was performed using a Cell Voyager 7000S automated system (Yokogawa, Tokyo, Japan) with a 20× objective. Seeded intracellular tau aggregates (CFP/YFP inclusions) were detected via a 488 nm laser (Ex: 460-490 nm, Em: 500-550 nm), and Hoechst-stained nuclei via a 405 nm laser (Ex: 360-400 nm, Em: 410-480 nm). Typically, 10-15 randomly selected fields per well were imaged. Image analysis was performed using inbuilt scripts in Signals Image Artist (Revvity, formerly PerkinElmer) to quantify cell number (number of Hoechst-positive cells) and the number of seeded intracellular tau aggregates (CFP/YFP inclusion) per well, as described before (14).

Statistical analysis

All data analyses and plotting were performed using GraphPad Prism (San Diego, CA). Results are shown as mean ± SEM, with statistical significance at $p < 0.05$.

Results

Tau-repeat peptides form fibrils with distinct aggregation kinetics and morphologies, including Thioflavin T-negative species

We employed three synthetic tau peptides: R2R3, R1R3, and R3R4. These constructs enabled systematic evaluation of the amyloidogenic motifs VQIINK (repeat R2) and VQIVYK (repeat R3), along with native cysteine residues implicated in oxidative crosslinking (Figure 1a). The R3R4 construct additionally includes the KKIET motif (residues 369-373) (Figure 1a), identified as part of the C-terminal region of tau amyloid fibrils' core derived from AD brain tissue (3).

Aggregation kinetics monitored by ThT fluorescence in heparin-supplemented aggregation buffer showed that R2R3 aggregated rapidly, plateauing within 24 h at 25 μM and 50 μM (Figure 1b). In contrast, R1R3 exhibited delayed and weaker ThT fluorescence at 48 h for the 50 μM concentration, whereas R3R4 showed no detectable ThT fluorescence within the same timeframe (Figure 1b). However, both R1R3 (at 25 and 50 μM) and R3R4 (at 50 μM) eventually reached fluorescence plateaus, albeit with low signal intensities, after extended incubation for 168 h (Figure 1c). None of the peptides showed a measurable ThT signal within 48 h without heparin (Figure S1).

AFM confirmed fibril formation for all three constructs, including R1R3 and R3R4, despite their weak ThT fluorescence signals, even at 48 h of aggregation (Figure 1d). Morphological differences

were observed, with R2R3 forming dense fibrils and R1R3/R3R4 forming thinner, more dispersed fibrils. ANS fluorescence assays revealed an early and substantial increase in signal for R2R3, with delayed and weaker responses for R1R3 and R3R4 (Figure 1e), indicating differences in the kinetics of hydrophobic surface exposure among the peptides.

R2R3 preferentially forms β-sheet-rich aggregates and exhibits stronger biochemical signatures of aggregation

To better understand sequence-dependent aggregation tendencies, we first analyzed the hydropathicity profiles of the peptides using the Kyte-Doolittle scale (15). R2R3 and R1R3 displayed strong hydrophilic mid-regions (residues 7-23 and 17-28, respectively), while R3R4 showed a more hydrophobic N-terminal stretch (residues 4-6) (Table 1). Next, we biochemically characterized the peptide aggregates formed after 48 h of incubation. SDS-PAGE, followed by Coomassie staining, revealed monomeric and dimeric species for all peptides, with varying intensities (Figure 2a). Faint dimer bands were also observed at 0 h, likely reflecting minor aggregation during peptide reconstitution and handling. After 48 h, R2R3 samples exhibited a markedly reduced monomer signal and a reproducible diffuse smear (Figure 2a, Figure S3). Although the smear did not resolve into discrete high-molecular-weight (HMW) bands, it aligned with the aggregation kinetics and likely represents heterogeneous higher-order assemblies. In contrast, R1R3 and R3R4 showed sharper, well-defined bands with minimal smearing.

Western blotting with the RD4 antibody, which specifically recognizes the R2 epitope (VQIINKKLDLSNVQSK) (16), confirmed the presence of smeared HMW species exclusively in R2R3 samples (Figure 2b). No RD4 signal was observed for R1R3 or R3R4 despite aggregation confirmed by Coomassie staining (Figure 2c).

CD spectroscopy further differentiated the constructs by secondary structure content. R2R3 displayed a clear, concentration- and time-dependent transition from random coil to β-sheet-rich conformation at 48 h in the presence of heparin (Figure 2d). This transition was reproducible at both 5 and 10 μM concentrations and did not occur under quiescent conditions without heparin (Figure S4). In contrast, R1R3 and R3R4 retained predominantly random-coil structures throughout the same incubation period, regardless of heparin treatment or concentration (Figure 2d, Figure S4).

R2R3 fibrils efficiently seed intracellular aggregation and enable secondary propagation in biosensor cells

To determine the functional relevance of the synthetic tau repeat peptides as *in vitro* models for tau prion-like behavior, we assessed the seeding ability of their fibrils. Tau RD P301S FRET biosensor cells seeded with R2R3 fibrils (48 h aggregation) exhibited abundant intracellular FRET-positive aggregates, while R1R3 and R3R4 induced fewer inclusions (Figure 3a). Quantitative analysis confirmed significantly higher seeding activity for R2R3 fibrils formed after 48 h or 168 h of aggregation compared to R1R3 and R3R4 (Figure 3b, c). To test the potential of these seeded aggregates to propagate tau pathology further, we performed a secondary seeding assay. All fractions obtained from cells initially seeded with R2R3 fibrils effectively induced tau aggregation in naïve recipient cells, demonstrating propagation-competent tau seeds (Figure 3d). Conversely, fractions from cells seeded with R1R3 or R3R4 fibrils showed negligible secondary seeding activity, even when total lysates were used.

Discussion

This study establishes unmodified tau repeat peptides as a minimal model system for probing aggregation kinetics, fibril polymorphism, secondary structure, and seeding behavior. Among the three constructs tested, the R2R3 peptide demonstrated markedly faster aggregation kinetics, stronger ThT and ANS fluorescence signals, and robust β-sheet transition, setting it apart from the slower-aggregating R1R3 and R3R4 peptides. These findings align with prior structural studies demonstrating the strong amyloidogenic potential of VQIINK and VQIVYK motifs, capable of forming stable steric zipper interfaces and promoting rapid aggregation of full-length tau (12). The absence of detectable aggregation by ThT fluorescence under heparin-free conditions supports the conclusion that these tau peptides require polyanionic cofactors to efficiently nucleate fibril formation within early aggregation windows.

Despite their minimal or undetectable ThT fluorescence at early time points (48 h), AFM confirmed fibril formation by R1R3 and R3R4. This observation is consistent with previous reports by Chen et al., who showed that tauRD variants, such as those with the S320F mutation, form fibrils with substantially reduced ThT binding but retain cellular seeding activity (6). Our data extends this concept by showing that native R1R3 and R3R4 fragments also form fibrils less

reactive to ThT, emphasizing the importance of complementing ThT fluorescence with direct visualization methods when evaluating tau aggregation and polymorphism.

Marked differences in fibril morphology among the constructs were observed, with R2R3 forming dense, laterally clustered fibrils, whereas R1R3 and R3R4 generated thinner, more dispersed structures. These morphological variations likely reflect sequence-specific differences in fibril nucleation and assembly. Prior work demonstrated that engineered constructs with duplicated VQIINK motifs (2xIN) formed fibrils more rapidly than those with duplicated VQIVYK (2xVY) (12), but our findings expand this understanding to naturally adjacent repeat sequences, showing that combinations such as R2R3 confer additional aggregation advantages beyond the properties of isolated amyloidogenic motifs. In support of this, hydropathicity profiling revealed strong hydrophilic mid-regions in R2R3 and R1R3 and a hydrophobic N-terminal segment in R3R4, aligning with their respective aggregation behaviors and supporting the role of sequence-encoded hydrophobicity in tau peptide aggregation.

SDS-PAGE and Western blotting confirmed that only R2R3 forms SDS-resistant, higher-order aggregates. The diffuse smear observed in R2R3 lanes by Coomassie staining was also immunoreactive with RD4, indicating that these HMW species contain the R2 epitope and are consistent with aggregated tau conformers (16). This supports previous findings that the R2-R3 junction is a key driver of tau aggregation (4, 12). In contrast, R1R3 and R3R4 showed no comparable smear in Coomassie, and as expected, no RD4 signal, consistent with their lack of the R2 sequence and absence of similar HMW aggregate formation.

CD analysis further differentiated the constructs by secondary structure formation. Only R2R3 displayed a pronounced transition from random coil to β-sheet structure after 48 h in the presence of heparin, while R1R3 and R3R4 retained random-coil conformations. These results reinforce the idea that combining VQIINK and VQIVYK within R2R3 facilitates a rapid structural rearrangement conducive to aggregation. The R3R4 fragment, although containing the C-terminal core region observed in AD brain-derived fibrils (3), demonstrated slower kinetics and only modest hydrophobic surface exposure, supporting a model in which the R2R3 sequence promotes early aggregation events, potentially enhancing nucleation efficiency prior to amyloid core stabilization.

To further probe early conformational changes during aggregation, we used ANS fluorescence to assess hydrophobic surface exposure. The early increase in ANS fluorescence observed for R2R3 likely reflects conformational changes during aggregation that transiently expose hydrophobic residues, especially lysines, which enhance ANS binding. This interpretation aligns with prior work using TauRD constructs, where increased ANS signal was attributed to aggregation-induced structural rearrangements rather than classical hydrophobic unfolding (17). Supporting this view, hydropathicity profiling showed that R2R3 harbors a broad hydrophilic mid-region (residues 7-23), and its rapid conformational reorganization may render adjacent residues more accessible to ANS. In contrast, R3R4 contains a hydrophobic N-terminal segment (residues 4-6) that may become rapidly buried during nucleation, reducing ANS accessibility. R1R3 showed intermediate behavior consistent with its slower aggregation. Collectively, these data support a model where ANS fluorescence sensitively tracks early conformational dynamics shaped by sequence-encoded hydropathicity and residue accessibility.

Functionally, only R2R3 fibrils induced strong intracellular seeding in Tau RD P301S biosensor cells and enabled secondary propagation in recipient cells. These findings demonstrate that fibrils from R2R3 peptides not only efficiently nucleate initial intracellular aggregates but also generate tau species capable of reseeding aggregation upon transfer to naive cells - a hallmark characteristic of pathological tau prions (18). Despite their ability to form fibrils, R1R3 and R3R4 failed to induce secondary seeding under the conditions tested. We have previously shown that R2 and R3 peptides individually form amyloid fibrils that induce primary and secondary seeding in Tau RD P301S biosensor cells, along with AD-relevant phosphorylation of endogenous tau in cells expressing 0N4R P301L tau (14). In contrast, R1 and R4 show no such activity. Moreover, R2 fibrils exhibit a stronger and earlier seeding response than R3 under identical conditions, suggesting that R2 may play a dominant initiating role in tau pathology among the repeat domains (19). The R2R3 construct, by integrating two independently competent domains within a native sequence framework, thus provides a more robust and tractable system for modeling 4R tau aggregation and propagation.

Although R2R3 aggregates more rapidly and forms denser fibrils *in vitro*, Cryo-EM studies of tau filaments from AD brains consistently show that R3R4 comprises the structured fibril core (3). One possible explanation is that the laterally clustered fibrils formed by R2R3, as observed by our

AFM imaging, may be excluded during Cryo-EM sample preparation due to their size, heterogeneity, or poor dispersion (20, 21). Additionally, R3R4 may form a proteolytically stable core that is preferentially retained during disease progression or biochemical extraction (22). While our study did not directly assess protease resistance, future experiments comparing the susceptibility of R2R3 and R3R4 fibrils to proteolytic degradation could clarify this possibility. It is also plausible that R2R3 contributes to early nucleation events, with R3R4 being conformationally selected as a more stable end-state structure (21, 22). These possibilities underscore how structural maturation and context-dependent selection, whether driven by proteolytic processing, fibril stability, or experimental enrichment, may influence which tau regions become dominant in disease-associated fibril cores.

While our study emphasizes the value of R2R3 as a native, unmodified construct that captures key features of tau aggregation and propagation, we recognize that other minimal systems, including hexapeptides like VQIINK and VQIVYK, PHF43 peptide, and full-length tau (23), offer complementary models with different strengths and applications. Thus, R2R3 serves as a minimal model for probing aggregation mechanisms, particularly suited for evaluating sequence context effects and prion-like propagation in a controlled system.

Our work complements recent studies that demonstrated enhanced tau aggregation via lysine acetylation (9). However, unlike those chemically modified systems, our findings highlight the intrinsic aggregation potential of native tau sequences. The use of unmodified R2R3 establishes a baseline for understanding the sequence-encoded drivers of tau aggregation and provides a clean platform for future work investigating the additive or synergistic roles of post-translational modifications.

Taken together, these findings establish the unmodified R2R3 tau repeat peptide as a robust and mechanistically informative minimal model for tau aggregation and prion-like propagation. The construct exhibits a distinctive profile - rapid aggregation, early β-sheet conversion, and strong intracellular seeding and propagation activity, distinguishing it from other native repeat combinations. While the amyloidogenic potential of the VQIINK motif is well-documented (12), our study emphasizes that the native R2-R3 junction, without chemical modification, is sufficient to initiate tau fibrillization and yield propagation-competent seeds. This provides a critical reference point for future work exploring how post-translational modifications, such as lysine

acetylation (9), further modulate tau aggregation behavior. Although peptide models inherently lack the full complexity of native tau, such as its length, cellular modifications, and interactions within cells, they offer a well-defined and tractable system for studying sequence-driven aggregation mechanisms. In conclusion, the R2R3 construct offers a valuable platform for mechanistic studies and therapeutic screening targeting tauopathies.

Acknowledgments

The work was supported by the Grant Agency of the Czech Republic under Grant # 23-06301J and the National Institute for Neurological Research (Program EXCELES, ID Project No. LX22NPO5107), funded by the European Union - Next Generation EU through the Ministry of Education, Youth and Sports of the Czech Republic (MEYS) to V.D. Additional support was received from the infrastructural projects CZ-OPENSCREEN (LM2023052) and EATRIS-CZ (LM2023053), the Czech biobank network BBMRI (LM2023033), and the Czech-BioImaging (LM2023050, LM2018129) funded through the MEYS, and the project TN02000109 (Personalized Medicine: From Translational Research into Biomedical Applications) by the Technology Agency of the Czech Republic. Additionally, this work was supported by Fondazione Sacchetti (Grants 2022–2023 and 2024) to L.D. and M.M. and by FONDAZIONE REGIONALE PER LA RICERCA BIOMEDICA (Care4NeuroRare CP_20/ 2018) to L.D.

Author contributions

V.D.: Conceptualization, methodology, investigation, interpretation, funding acquisition, supervision, and writing – original draft, review, and editing. **L.D.**: Methodology, investigation, interpretation, and writing – review and editing. **LM**: Methodology and investigation. **M.M.**: Methodology, investigation, and writing – review and editing. **N.A.**: Methodology, investigation.

Declaration of interests

The authors declare no competing interests.

Data availability

The data supporting the findings of this study are openly available in Zenodo at DOI: 10.5281/zenodo.15119096. Any additional data are included within the article and its supplementary materials. The Zenodo repository contains raw datasets for Thioflavin T

fluorescence, 8-anilinonaphthalene-1-sulfonic acid fluorescence, circular dichroism spectra, and aggregate counts from seeding assays. For the seeding experiments, full statistical outputs - including F and degrees of freedom (DF) values for ANOVA—are included in the associated source data file.

Declaration of generative AI

While preparing this work, the authors used Grammarly to improve language. After using this tool, the authors reviewed and edited the content as needed and take full responsibility for the publication's content.

References

1. Goedert, M., M.G. Spillantini, R. Jakes, D. Rutherford, and R.A. Crowther. 1989. Multiple isoforms of human microtubule-associated protein tau: sequences and localization in neurofibrillary tangles of Alzheimer's disease. Neuron. 3.

2. Ganguly, P., T.D. Do, L. Larini, N.E. LaPointe, A.J. Sercel, M.F. Shade, S.C. Feinstein, M.T. Bowers, and J.-E. Shea. 2015. Tau Assembly: The Dominant Role of PHF6 (VQIVYK) in Microtubule Binding Region Repeat R3. J. Phys. Chem. B. 119:4582–4593.

3. Fitzpatrick, A.W.P., B. Falcon, S. He, A.G. Murzin, G. Murshudov, H.J. Garringer, R.A. Crowther, B. Ghetti, M. Goedert, and S.H.W. Scheres. 2017. Cryo-EM structures of tau filaments from Alzheimer's disease. Nature. 547:185–190.

4. Yang, J., M.V. Agnihotri, C.J. Huseby, J. Kuret, and S.J. Singer. 2021. A theoretical study of polymorphism in VQIVYK fibrils. Biophys. J. 120:1396–1416.

5. Chen, D., K.W. Drombosky, Z. Hou, L. Sari, O.M. Kashmer, B.D. Ryder, V.A. Perez, D.R. Woodard, M.M. Lin, M.I. Diamond, and L.A. Joachimiak. 2019. Tau local structure shields an amyloid-forming motif and controls aggregation propensity. Nat. Commun. 10:2493.

6. Chen, D., S. Bali, R. Singh, A. Wosztyl, V. Mullapudi, J. Vaquer-Alicea, P. Jayan, S. Melhem, H. Seelaar, J.C. van Swieten, M.I. Diamond, and L.A. Joachimiak. 2023. FTD-tau S320F mutation stabilizes local structure and allosterically promotes amyloid motif-dependent aggregation. Nat. Commun. 14:1625.

7. Soeda, Y., M. Yoshikawa, O.F.X. Almeida, A. Sumioka, S. Maeda, H. Osada, Y. Kondoh, A. Saito, T. Miyasaka, T. Kimura, M. Suzuki, H. Koyama, Y. Yoshiike, H. Sugimoto, Y. Ihara, and A. Takashima. 2015. Toxic tau oligomer formation blocked by capping of cysteine residues with 1,2-dihydroxybenzene groups. Nat. Commun. 6:10216.

8. Lövestam, S., D. Li, J.L. Wagstaff, A. Kotecha, D. Kimanius, S.H. McLaughlin, A.G. Murzin, S.M.V. Freund, M. Goedert, and S.H.W. Scheres. 2024. Disease-specific tau filaments assemble via polymorphic intermediates. Nature. 625:119–125.

9. Li, L., B.A. Nguyen, V. Mullapudi, Y. Li, L. Saelices, and L.A. Joachimiak. 2023. Disease-associated patterns of acetylation stabilize tau fibril formation. Structure. 31:1025-1037.e4.

10. Aillaud, I., and S.A. Funke. 2023. Tau Aggregation Inhibiting Peptides as Potential Therapeutics for Alzheimer Disease. Cell. Mol. Neurobiol. 43:951–961.

11. Tsuchida, T., K. Susa, T. Kibiki, T. Tsuchiya, K. Miyamoto, Y. In, K. Minoura, T. Taniguchi, T. Ishida, and K. Tomoo. 2020. Crystal structure of the human tau PHF core domain VQIINK complexed with the Fab domain of monoclonal antibody Tau2r3. FEBS Lett. 594:2140–2149.

12. Seidler, P.M., D.R. Boyer, J.A. Rodriguez, M.R. Sawaya, D. Cascio, K. Murray, T. Gonen, and D.S. Eisenberg. 2018. Structure-based inhibitors of tau aggregation. Nat. Chem. 10:170–176.

13. Lövestam, S., J.L. Wagstaff, T. Katsinelos, S.M. Freund, M. Goedert, and S.H. Scheres. 2025. Twelve phosphomimetic mutations induce the assembly of recombinant full-length human tau into paired helical filaments. .

14. Annadurai, N., L. Malina, J. Malohlava, M. Hajdúch, and V. Das. 2022. Tau R2 and R3 are essential regions for tau aggregation, seeding and propagation. Biochimie. 200:79–86.

15. Kyte, J., and R.F. Doolittle. 1982. A simple method for displaying the hydropathic character of a protein. J. Mol. Biol. 157:105–132.

16. Togo, T., N. Sahara, S.-H. Yen, N. Cookson, T. Ishizawa, M. Hutton, R. de Silva, A. Lees, and D.W. Dickson. 2002. Argyrophilic Grain Disease Is a Sporadic 4-Repeat Tauopathy. J. Neuropathol. Exp. Neurol. 61:547–556.

17. Kumar, S., K. Tepper, S. Kaniyappan, J. Biernat, S. Wegmann, E.-M. Mandelkow, D.J. Müller, and E. Mandelkow. 2014. Stages and Conformations of the Tau Repeat Domain during Aggregation and Its Effect on Neuronal Toxicity. J. Biol. Chem. 289:20318–20332.

18. Wang, J., C.K. Williams, M.A. DeTure, S.D. Magaki, D.W. Dickson, H.V. Vinters, and P.M. Seidler. 2024. Tau seeds catalyze fibril-type structures from GFP tau biosensor cells. Structure. 32:2251-2258.e3.

19. Annadurai, N., J. Hrubý, A. Kubíčková, L. Malina, M. Hajdúch, and V. Das. 2023. Time- and dose-dependent seeding tendency of exogenous tau R2 and R3 aggregates in cells. Biochem. Biophys. Res. Commun. 653:102–105.

20. Zhang, W., B. Falcon, A.G. Murzin, J. Fan, R.A. Crowther, M. Goedert, and S.H. Scheres. 2019. Heparin-induced tau filaments are polymorphic and differ from those in Alzheimer's and Pick's diseases. eLife. 8:e43584.

21. Falcon, B., W. Zhang, A.G. Murzin, G. Murshudov, H.J. Garringer, R. Vidal, R.A. Crowther, B. Ghetti, S.H.W. Scheres, and M. Goedert. 2018. Structures of filaments from Pick's disease reveal a novel tau protein fold. Nature. 561:137–140.

22. Arakhamia, T., C.E. Lee, Y. Carlomagno, M. Kumar, D.M. Duong, H. Wesseling, S.R. Kundinger, K. Wang, D. Williams, M. DeTure, D.W. Dickson, C.N. Cook, N.T. Seyfried, L. Petrucelli, J.A. Steen, and A.W.P. Fitzpatrick. 2020. Posttranslational Modifications Mediate the Structural Diversity of Tauopathy Strains. Cell. 180:633-644.e12.

23. von Bergen, M., P. Friedhoff, J. Biernat, J. Heberle, E.-M. Mandelkow, and E. Mandelkow. 2000. Assembly of τ protein into Alzheimer paired helical filaments depends on a local sequence motif ((306)VQIVYK(311)) forming β structure. PNAS. 97:5129–5134.

Table 1. Hydropathicity profiles of tau repeat peptides calculated using the Kyte-Doolittle scale. The minimum and maximum hydropathicity values, their respective residue positions, and the regions of notable hydrophobic or hydrophilic character are shown for each peptide. Hydropathicity values were obtained using the ExPASy ProtScale tool.

Peptide	Min Hydropathicity	Max Hydropathicity	Position of Min	Position of Max	Hydrophobic Peak Region	Strongly Hydrophilic Region
R2R3	-1.978	0.678	17	31	29-37	7-23
R1R3	-1.878	0.622	22	37	30-37	17-28
R3R4	-1.889	0.622	39	6	4-6	38-43

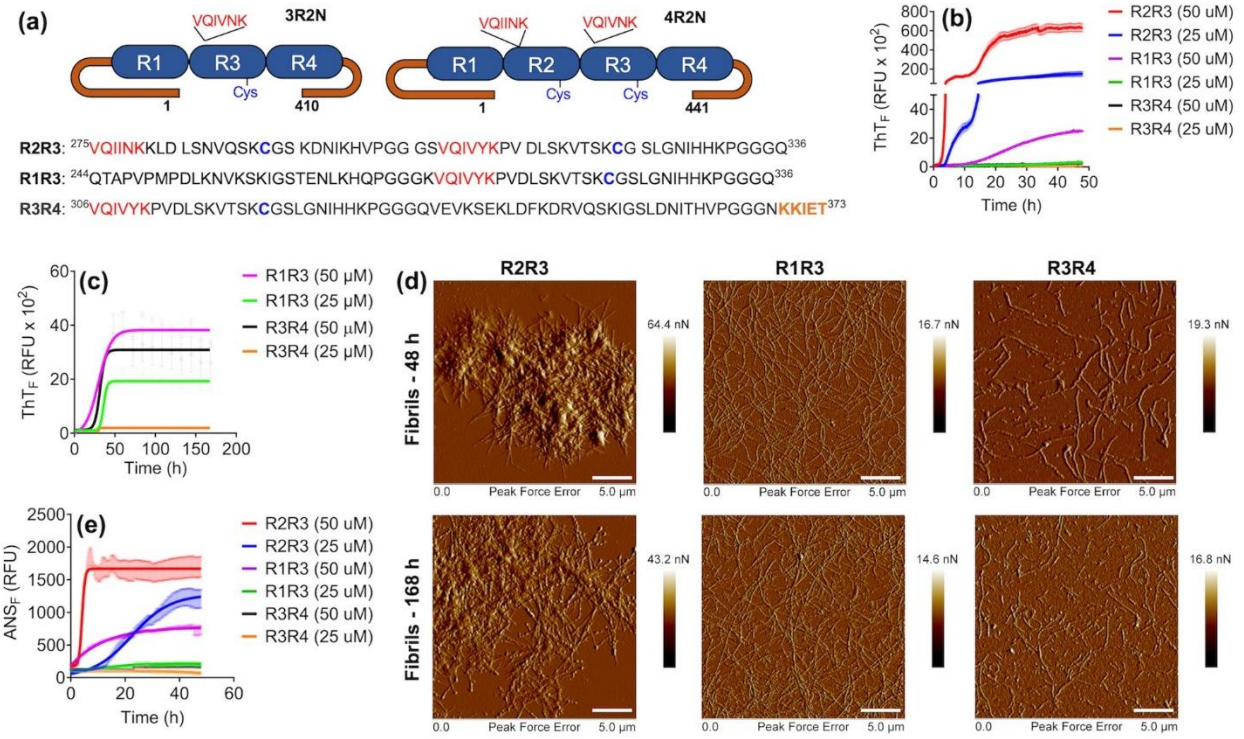

Figure 1. **Aggregation and structural properties of tau repeat peptides**. (**a**) Schematic representation of 3R and 4R tau isoforms showing the microtubule-binding repeats (R1-R4), amyloid motifs (red), and cysteine residues. Below: Amino acid sequences of R2R3, R1R3, and R3R4 peptide constructs. The amyloid motifs are highlighted in red, cysteine residues in blue, and the 'KKIET' sequence (residues 369-373 in R4), which forms part of the core of AD filaments, in orange. (**b**) Aggregation kinetics of R3R4, R1R3, and R2R3 peptides at 25 µM and 50 µM over 48 h, monitored using ThT fluorescence. Mean ± SEM (n = 4 independent replicates). (**c**) Long-term aggregation kinetics of R1R3 and R3R4 over 168 h. Mean ± SEM (n = 3 independent replicates). (**d**) AFM images showing peptide morphology after 48 h and 168 h of aggregation, confirming fibril formation. (**e**) ANS fluorescence kinetics assay, assessing hydrophobic exposure during peptide aggregation over 48 h. Increased fluorescence indicates structural transitions and early aggregation events. Mean ± SEM (n = 4 independent replicates). Information on source data is available in the Data Availability section.

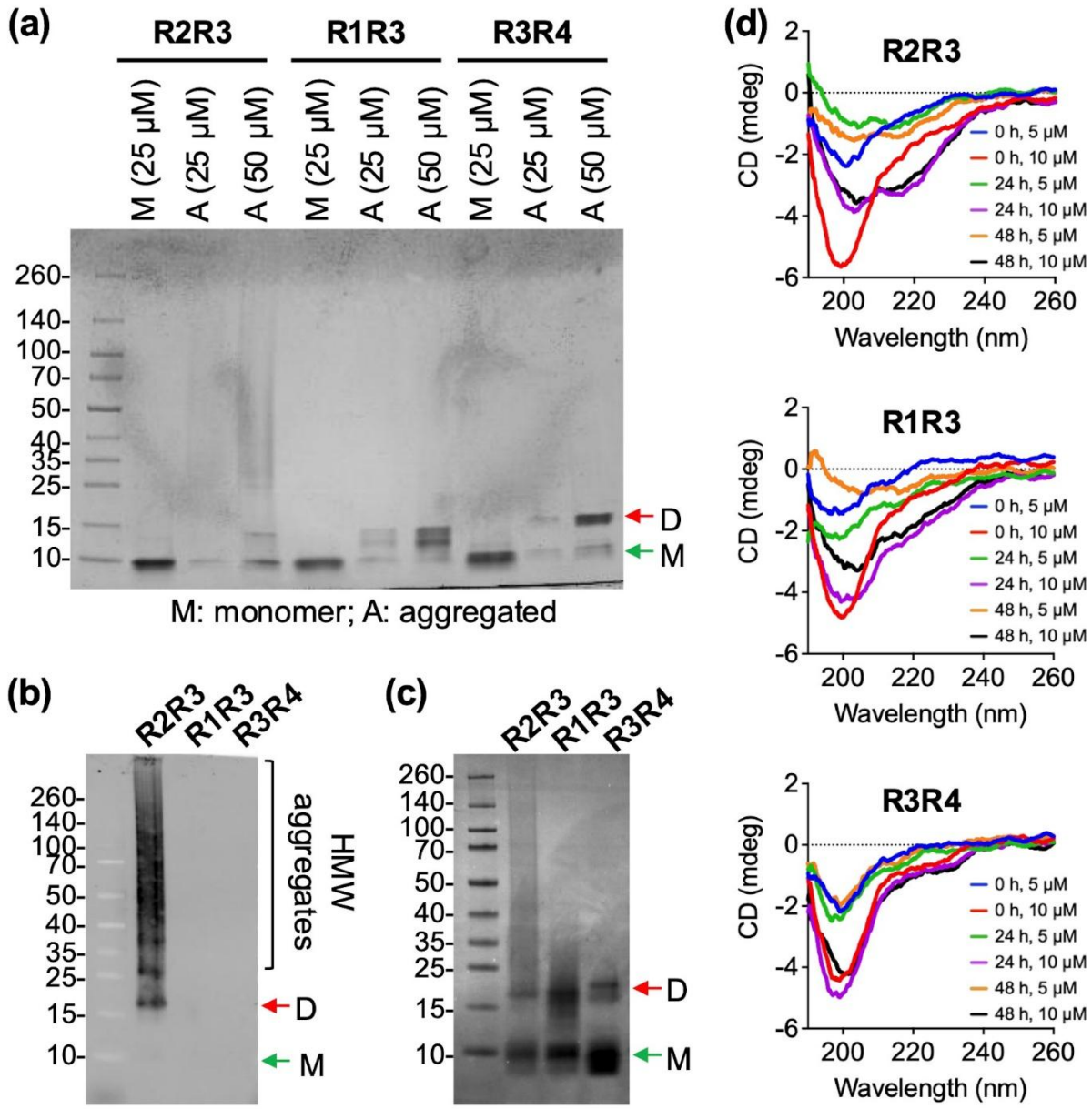

Figure 2. Biochemical validation and conformational analysis of peptide aggregates. (**a**) Coomassie-stained SDS-PAGE gel showing monomer and dimer bands across all peptides after 48 h of aggregation. A diffuse smear is visible in R2R3 lanes, indicative of higher-order aggregate formation. Similar patterns were observed in independent replicates (see Figure S2). (**b**) Western blot with anti-4R tau RD4 antibody after 48 h of aggregation, showing dimer and HMW species in only R2R3. (**c**) Coomassie-staining of the same samples, confirming aggregation in the loaded samples. (**d**) CD spectra of peptides at 5 and 10 µM, diluted in 10 mM phosphate buffer (pH 6.8) with heparin (peptide: heparin at a 5:1 molar ratio), recorded at 0 h, 24 h, and 48 h at 37°C.

Information on source data is available in the Data Availability section. Images of replicate Coomassie-stained gels for panel (a) and the uncropped Western blot and Coomassie gels in panels (c, d) are provided in the Supplementary Material. Arrows indicate monomer (M) and dimer (D) bands.

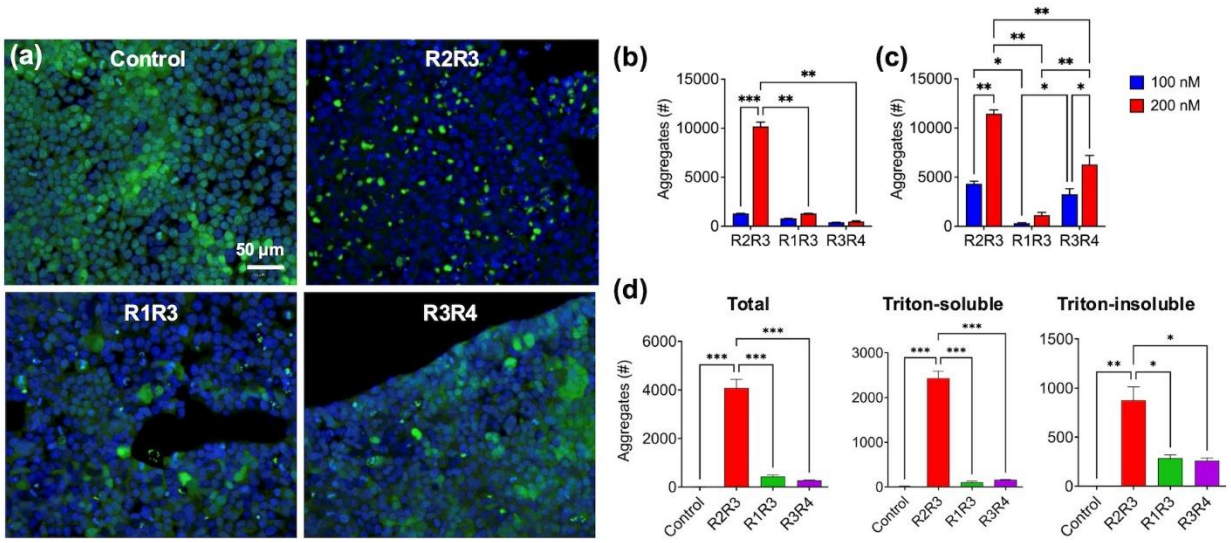

Figure 3. Seeding competency of peptide aggregates. (**a**) Confocal microscopy images of tau RD P301S FRET biosensor cells transduced with peptide fibrils aggregated for 48 h. Seeded intracellular tau aggregates appear as green FRET-positive inclusions (CFP/YFP signal). Nuclei are counterstained with Hoechst-33342 (blue). (**b**, **c**) Quantification of intracellular tau aggregation following treatment with peptide fibrils collected after 48 h (b) and 168 h (c) of aggregation. (**d**) Quantification of FRET-positive inclusions in biosensor cells transduced with the total, Triton-soluble, and Triton-insoluble fractions derived from cells previously seeded with either buffer (heparin only, Control) or fibrils of R2R3, R1R3, and R3R4 collected at 48 h. All data represent mean ± SEM (n = 2 independent replicates). ***p ≤ 0.001, **p ≤ 0.01, *p ≤ 0.05, two-way ANOVA (b, c) and one-way ANOVA (d) followed by Tukey's multiple comparisons *post hoc* test. Information on source data and corresponding F and degrees of freedom (DF) values for ANOVA are provided in the Data Availability section.